

Case History

Improved resolution in Bayesian lithology/fluid inversion from prestack seismic data and well observations: Part 2 — Real case study

Marit Ulvmoen¹, Henning Omre¹, and Arild Buland²

ABSTRACT

We have performed lithology/fluid inversion based on prestack seismic data and well observations from a gas reservoir offshore Norway. The prior profile Markov random field model captures horizontal continuity and vertical sequencing of the lithology/fluid variables. The prior model is also locally adjusted for spatially varying lithology/fluid proportions. The likelihood model is inferred from basic seismic theory and observations in wells. An approximate posterior model is defined, which can be simulated from by an extremely computer-efficient algorithm. The lithology/fluid inversion results are compared to manual interpretations and evaluated by cross validation in one well. Moreover, inversions based on simplified prior models are developed for comparative reasons. Both lithology/fluid realizations and predictions look geologically reasonable. The results seem to reflect general reservoir experience and information provided by the prestack seismic data and well observations. The lithology/fluid proportions appear as geologically plausible and thin elongated lithology/fluid units are identified. The study is made in a 2D cross section, but extension to a full 3D setting is feasible.

INTRODUCTION

Prediction of lithology/fluid (LF) characteristics is important in development of petroleum reserves, both at the exploration and production stage. In an exploration setting, the information available is often limited to seismic data and geologists' knowledge about the area. In a production setting, both seismic and well data are available.

The objective of the study is to infer LF classes in a gas reservoir offshore Norway in a production setting, using prestack, true-amplitude imaged seismic data and well observations. The inversion pro-

cedure is defined in a Bayesian setting. In this setting, prior information about the LF characteristics is combined with likelihood models linking the observed data to the characteristics, and the complete solution is the posterior model. The procedure follows the methodology defined in [Ulvmoen and Omre](#) (this issue), where an approach for LF inversion is defined. In that paper, the inversion approach is evaluated on synthetic data, with all model parameters known. Real data are used in this study, which introduces several new challenges. The likelihood part of the Bayesian model is divided into three likelihood models. Observations from wells are used in inference of these models; hence the existence of at least one well in the target zone or surrounding area is of great importance.

The prior model for the categorical LF variables should capture characteristics of the variables and must be based on general reservoir experience. Lithologies are created by sedimentary processes and are expected to appear as thin, elongated units, and fluids will be gravitationally segregated. Layers of shale are particularly important because they have a large impact on fluid flow. A profile Markov random field prior model is used to represent these features.

Several papers on LF inversion of seismic data use spatially coupled models for the LF variables. [Eidsvik et al. \(2004\)](#) present a 2D study in a geologic horizon based on a traditional Markov random field prior model for shale/sand and fluids. The seismic deconvolution was avoided because only peak reflections were used. In [Contreras et al. \(2005\)](#), a multivariate approach to fluid unit inversion of real data is presented. The model used is continuous and Gaussian. [Buland et al. \(2008\)](#) present a 3D study with deconvolution and vertical coupling in the model for the elastic material variables. No spatial prior was defined for the LF variables themselves. In [González et al. \(2008\)](#), a multipoint prior model is defined on the LF variables, but conditioning on seismic data is made only in an ad hoc manner. In [Bosch et al. \(2009\)](#), porosity and saturation are inferred from stacked seismic data and well observations. Consequently, the current study appears as the first that includes a formal horizontally/vertically coupled categorical model for the LF variables. Moreover, deconvolution of AVO seismic data is an integrated part of the inversion process.

Manuscript received by the Editor 9 February 2009; revised manuscript received 2 June 2009; published online 1 April 2010.

¹Norwegian University of Science and Technology, Trondheim, Norway. E-mail: ulvmoen@math.ntnu.no; omre@math.ntnu.no.

²StatoilHydro, Stavanger, Norway. E-mail: abu@statoil.com.

© 2010 Society of Exploration Geophysicists. All rights reserved.

The primary objective of the study is to demonstrate the methodology defined in [Ulvmoen and Omre](#) (this issue) on a real case study. The steps in the LF inversion approach are (1) define variables of interest and reference discretization over the reservoir; (2) define a well likelihood model that links well observations with variables of interest; (3) define seismic and rock-physics likelihood models that link seismic AVO data with variables of interest; (4) assess a prior model for variables of interest; and (5) combine the models above to define the posterior model for variables of interest given well and seismic information. Lastly, realizations from the posterior model are generated by a Markov chain Monte Carlo (MCMC) algorithm to assess predictions with associated uncertainties of the LF characteristics. The major findings are (1) posterior models based on spatially coupled categorical prior models for the LF characteristics provide realistic reservoir predictions; (2) resolution in the predictions appears to be improved relative to nonspatial models; and (3) computational demands of the algorithm are such that evaluation of 3D reservoirs is within reach.

MODEL INFERENCE

The 2D target zone is a sandstone reservoir offshore Norway. Both prestack seismic data (Figure 1) and observations from one well (Figure 2) are available in the target zone. The existence of gas in some sandstone layers is established in the well. The target zone is discretized and divided into lateral horizons and vertical profiles. Vertical profiles are discretized downward in $t \in \{1, \dots, T\}$, where the reflection time t corresponds to the seismic sampling. The lateral horizons are further discretized in seismic survey positions. In Figure 1, the target zone is defined within the upper and lower solid lines. These lines are parallel to the base Cretaceous unconformity (BCU), which can be identified as the clear reflection approximately 32 ms below the upper solid line. The seismic data in the target zone

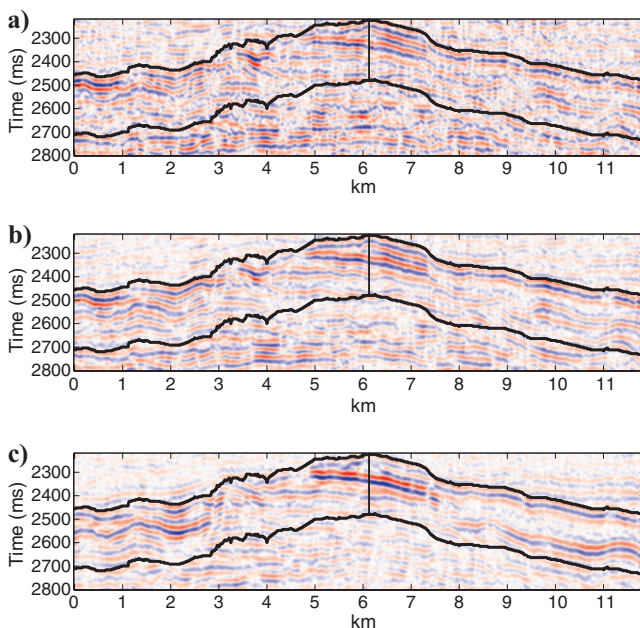


Figure 1. Prestack seismic data \mathbf{d}^s for angles $\theta = (10^\circ, 21^\circ, 36^\circ)$ in (a), (b) and (c), respectively, with the three seismic sections equally scaled. The inversion window is defined between the black lines, and the well location is marked as the vertical line.

are aligned to the BCU such that a rectangular field is inverted; hence the lithologies are given continuity parallel to the BCU horizon. The seismic data \mathbf{d}^s in Figure 1 range from 2220 ms to 2800 ms, with samples every 4 ms collected for the angles $\theta = (10^\circ, 21^\circ, 36^\circ)$. The data have been true-amplitude processed and prestack time migrated by a processing contractor. The quality of the seismic data is considered to be good, but with some residual moveout. We use 950 profiles and a 260-ms time window; hence $T = 65$ as the seismic data are sampled every 4 ms.

The well location is marked in Figure 1. Well observations \mathbf{d}^w in Figure 2 have been depth-to-time converted such that the well sampling coincides with the seismic sampling. The original well observations are on a finer resolution, and are upsampled by selecting the subset of observations corresponding to node locations. In addition to the gas layers, the well contains a layer of source rock directly below the BCU and several thin layers of brine in sandstone layers. The BCU is overlaid by a thick layer of shale, and shale is also found between layers of sandstone and source rock. Based on the observations in the well, the target zone is assumed to consist of three lithologies: Sandstone, shale, and source rock. Sandstone is saturated with either gas or brine. This defines four LF classes in the inversion. The proportions of the lithologies in the well are about 0.45, 0.5, and 0.05 for sandstone, shale, and source rock, respectively. The joint set of well observations and seismic data is denoted by $\mathbf{d} = \{\mathbf{d}^w, \mathbf{d}^s\}$.

The complete set of LF classes in the target zone is denoted by $\boldsymbol{\pi}$: $\{\pi_{x,t}; \text{all } (x,t)\}$, with $\pi_{x,t}$ being the LF class in lattice node (x,t) . Each $\pi_{x,t}$ can take one of the four LF classes (gas-saturated sandstone, brine-saturated sandstone, shale, or source rock) such that $\pi_{x,t} \in \{\text{SG, SB, SH, SR}\}$. The LF characteristics $\boldsymbol{\pi}$ are the focus of this study.

In addition to observations of LF classes, the well contains observations of the three elastic material properties, P-wave velocity, S-wave velocity, and density, along the well trace (see Figure 2). The logarithm of these variables in the target zone is denoted by \mathbf{m} : $\{\mathbf{m}_{x,t}; \text{all } (x,t)\}$, with $\mathbf{m}_{x,t}$ representing the log transform of the three elastic

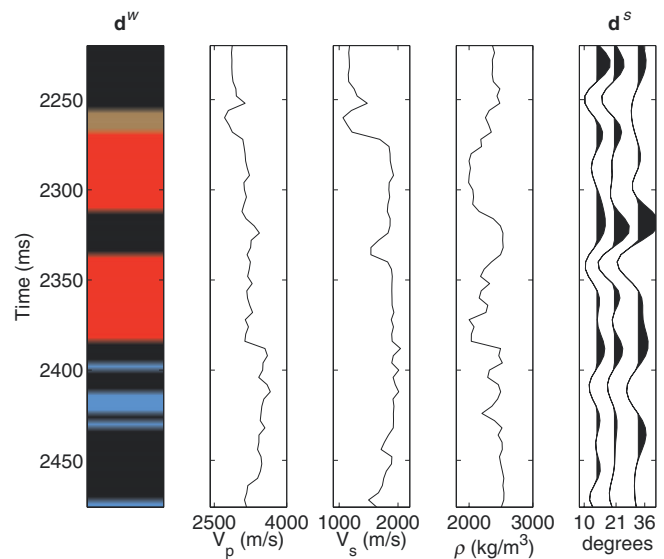


Figure 2. Well observations \mathbf{d}^w of LF classes with gas-saturated sandstone (red), brine-saturated sandstone (blue), shale (black), and source rock (brown); elastic material properties P-wave velocity V_p , S-wave velocity V_s , and density ρ ; and seismic data \mathbf{d}^s in well location.

variables in lattice node (x, t) . The original well observations are on a finer resolution, and are upsampled by selecting the subset of observations corresponding to node locations.

In [Ulvmoen and Omre](#) (this issue), the inversion approach is defined in a Bayesian setting where the complete solution is the posterior model defined by

$$p(\boldsymbol{\pi}|\mathbf{d}) = \text{const} \times p(\mathbf{d}^w|\boldsymbol{\pi})p(\mathbf{d}^s|\boldsymbol{\pi})p(\boldsymbol{\pi}), \quad (1)$$

where $p(\mathbf{d}^w|\boldsymbol{\pi})$ is a well likelihood model, $p(\mathbf{d}^s|\boldsymbol{\pi})$ is a likelihood model for the seismic data, $p(\boldsymbol{\pi})$ is the prior model for the LF classes, and const is a normalizing constant. The constant is defined by the sum over all possible configurations of the LF classes in the target zone; hence direct calculation is extremely difficult. The elastic material properties are included in the model by rewriting the likelihood model for the seismic data as

$$p(\mathbf{d}^s|\boldsymbol{\pi}) = \int \cdots \int p(\mathbf{d}^s|\mathbf{m})p(\mathbf{m}|\boldsymbol{\pi})d\mathbf{m}, \quad (2)$$

where $p(\mathbf{d}^s|\mathbf{m})$ is a seismic likelihood model and $p(\mathbf{m}|\boldsymbol{\pi})$ is a rock-physics likelihood model. The integral is over all possible configurations of the three elastic variables in the target zone; hence it is computationally demanding to calculate.

Likelihood model

The likelihood model links the observations (i.e., well observations and seismic data) to the variables of interest, which are the LF classes.

The well observations \mathbf{d}^w (see [Figure 2](#)) are considered to be exact observations of LF classes along the well profile; hence the well likelihood model $p(\mathbf{d}^w|\boldsymbol{\pi})$ is a Dirac function in the well location, defined by

$$[d_{x,t}^w|\boldsymbol{\pi}_{x,t}] = \boldsymbol{\pi}_{x,t}. \quad (3)$$

Note that the well likelihood model is defined at the well location only.

The seismic likelihood model $p(\mathbf{d}^s|\mathbf{m})$ is defined by a convolved linearized Zoeppritz model given by

$$[\mathbf{d}^s|\mathbf{m}] = \mathbf{WADm} + \mathbf{e}, \quad (4)$$

where \mathbf{W} is a block-diagonal convolution matrix containing one wavelet for each time-angle gather, \mathbf{A} is a matrix of angle-dependent Aki-Richards coefficients, \mathbf{D} is a differential matrix giving the contrasts of the elastic material properties in \mathbf{m} , and \mathbf{e} is Gaussian error. The wavelets in \mathbf{W} , provided by the data owner, are shown in [Figure 3](#). We assume the error term to be a mixture of wavelet colored and white noise given by $\mathbf{e} = \mathbf{W}\mathbf{e}_c + \mathbf{e}_d$. The reflection noise is given variance $\sigma_{e_c}^2 = 0.0001$ while the observation noise is estimated from the well and seismic data to be $\sigma_{e_d}^2 = 1.3 \times 10^5$ following the methodology in [Buland and Omre \(2003b\)](#). The resulting signal-to-noise ratio between elastic parameters and observations is approximately two. Note that the total observation-error variance is on the same order of magnitude as the amplitude in the seismic data. The seismic likelihood model is rephrased as

$$p(\mathbf{d}^s|\mathbf{m}) = \text{const} \times \frac{p_*(\mathbf{m}|\mathbf{d}^s)}{p_*(\mathbf{m})}, \quad (5)$$

where $p_*(\mathbf{m}|\mathbf{d}^s)$ and $p_*(\mathbf{m})$ are Gaussian posterior and prior models in linearized Zoeppritz inversion (see [Buland and Omre, 2003a](#)). The Gaussian probability $p_*(\mathbf{m})$ is parametrized by $(\boldsymbol{\mu}_*, \boldsymbol{\Sigma}_*, c_*(\boldsymbol{\tau}))$ vertically, representing expectation, covariance, and spatial correlation function, respectively. These values are estimated from the observations of P-wave velocity, S-wave velocity, and density in the well (see [Figure 2](#)) by standard statistical estimators. Estimated values are fully specified in [Appendix A](#). Note that the model used is very general and does not overfit the observations in the well. The Gaussian posterior probability $p_*(\mathbf{m}|\mathbf{d}^s)$ is calculated from the associated linearized Zoeppritz deconvolution. An approximation as defined in [Ulvmoen and Omre](#) (this issue) is used to obtain $\tilde{p}(\mathbf{d}^s|\mathbf{m})$, which is in factorial form.

An empirical rock-physics model $p(\mathbf{m}|\boldsymbol{\pi})$ is used in the study. We use two wells from the target zone and surrounding area. These wells contain locationwise (based on location) observations of both LF classes and elastic variables; hence samples $[\mathbf{m}_{x,t}|\boldsymbol{\pi}_{x,t}]$ are available. The empirical rock-physics likelihood model,

$$p(\mathbf{m}|\boldsymbol{\pi}) = \prod_{x,t} p(\mathbf{m}_{x,t}|\boldsymbol{\pi}_{x,t}), \quad (6)$$

is defined from the well logs (see [Figure 4](#)). The LF classes are well separated and the pattern corresponds with rock physical theory (see [Avseth et al., 2005](#)). The source rock also is easily identified. It is encouraging that observations from two wells in the same reservoir, but still far apart, coincide so well.

Prior model

The prior model for the LF variables should capture the general characteristics of the variables and must be based on general reservoir experience. Because lithologies are created by sedimentary processes, they are expected to appear as relatively thin, elongated units. The fluids will, at an initial state, be horizontally continuous and gravitationally segregated, which entails that brine cannot be immediately above gas. These characteristics should be captured in the prior model. The profile Markov random field defined in [Ulvmoen and Omre](#) (this issue) can model the effects listed above. The mathematical expression for this type of Markov random field is

$$p(\boldsymbol{\pi}_x|\boldsymbol{\pi}_{-x}) = p(\boldsymbol{\pi}_x|\boldsymbol{\pi}_y; y \in \delta(x)); \text{ all } x, \quad (7)$$

where $\boldsymbol{\pi}_x$ is a vertical LF profile, $\boldsymbol{\pi}_{-x}$ is the set of all LF profiles except $\boldsymbol{\pi}_x$, and $\delta(x)$ is a fixed horizontal neighborhood around x . Fur-

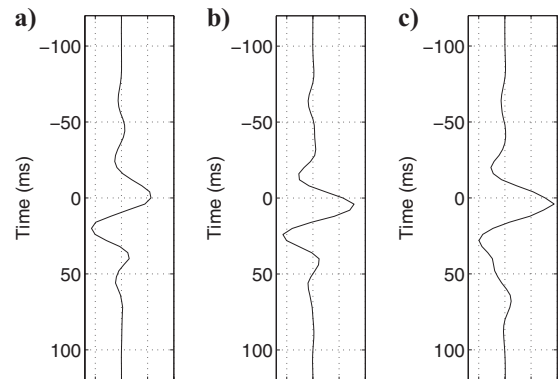


Figure 3. Wavelets used in inversion for angles $\theta = (10^\circ, 21^\circ, 36^\circ)$, in (a), (b), and (c), respectively.

ther, the LF profiles π , follow Markov chain models upward through the target zone (see [Ulvmoen and Omre](#), this issue)

$$p(\pi_x | \pi_y; y \in \delta(x)) = \prod_t p(\pi_{x,t} | \pi_{x,t+1}, \pi_{y,t}; y \in \delta(x)); \text{ all } x, \tag{8}$$

with $p(\pi_{x,t} | \pi_{x,t+1}, \pi_{y,t}; y \in \delta(x)) = p(\pi_{x,t} | \pi_{y,t}; y \in \delta(x))$ for notational convenience. This prior model is termed a 2D Markov random field model.

To fully specify the model, the elements in the transition matrix $p(\pi_{x,t} | \pi_{x,t+1}, \pi_{y,t}; y \in \delta(x))$ must be defined for all vertical configurations of $[\pi_{x,t}, \pi_{x,t+1}]$ and all lateral neighborhoods $\{\pi_{y,t}; y \in \delta(x)\}$. Transitions $[\pi_{x,t} | \pi_{x,t+1}]$ characterize the vertical dependence in the LF variables and are used to ensure gravity segregation of fluids. Lateral neighbors in $\{\pi_{y,t}; y \in \delta(x)\}$ ensure the horizontal dependence of both lithologies and fluids.

Basic elements in the transition matrices have the format

$$P'_{SG,SH} = \begin{pmatrix} 0.4999 & 0 & 0.4999 & 0.0002 \\ 0.4998 & 0.0002 & 0.4998 & 0.0002 \\ 0.4998 & 0.0002 & 0.4998 & 0.0002 \\ 0.4998 & 0.0002 & 0.4998 & 0.0002 \end{pmatrix},$$

with rows and columns appearing in the following order: gas-satu-

rated sandstone, brine-saturated sandstone, shale, and source rock. A closest horizontal neighborhood is used, and the subindices of P' indicate the neighboring class; hence the transition matrix presented above is the one with lateral neighbors being gas-saturated sandstone and shale. Note that brine immediately above gas is avoided by having the zero element in the matrix. Moreover, there is a high probability of having a class identical to one of the horizontally neighboring classes. If the neighbors are identical, this probability is very close to one. All the 10 basic transition matrices are fully specified in Appendix B. We have constructed these basic transition matrices to enforce lateral continuity on the LF variables and to ensure vertical fluid ordering. If the 10 basic transition matrices are averaged and the corresponding limiting distribution is computed, one obtains 0.27, 0.19, 0.27, 0.27. This distribution can be seen as an approximation of the prior proportions on gas-saturated sandstone, brine-saturated sandstone, shale, and source rock, defined by the prior model. Note that these proportions deviate from the lithology proportions observed in the well. Later we will present an approach for including spatially varying proportions. In principle, the transition matrices could be estimated from outcrop or training images by a simple counting process.

Experience from similar reservoir environments tells that the lithologies occur in different proportions in various layers of the reservoir. The expected proportions in the reservoir are displayed in Figure 5. The expected proportion of sandstone is 0.45, and constant across the reservoir. Shale and source rock tend to replace each other.

Above BCU source rock is highly unlikely, while it is abundant just below BCU. Further down from BCU shale is more common.

Fluids substitute each other in the sandstone lithology. Fluid contacts are known to be largely horizontal, and given the gas/brine contact in the well the contact level is assumed to be between 2380 and 2400 ms, and an expected saturation map can be specified (see Figure 6).

The basic transition matrices are adjusted in every node to accommodate the proportion maps in Figures 5 and 6. The adjustment procedure is defined in Appendix C. Correction factors are computed relative to the average of the basic transition matrices and they are enforced in a hierarchical manner. First, the proportions of sandstone versus shale/source rock are adjusted; thereafter gas/brine substitution in sandstone and shale/source rock substitution are made. This local adjustment of LF proportions is approximate (see Appendix C) but after thorough evaluation, we consider it to be reliable in our case study.

To compare posterior models for LF characteristics based on different prior models, the following alternative simplified prior models are defined:

- 1) A profilewise (based on profile) Markov chain prior model that ignores horizontal dependence between the vertical profiles. The average of the basic transition matrices given in Appendix B is used, with proportion adjustment for spatially varying LF proportions.

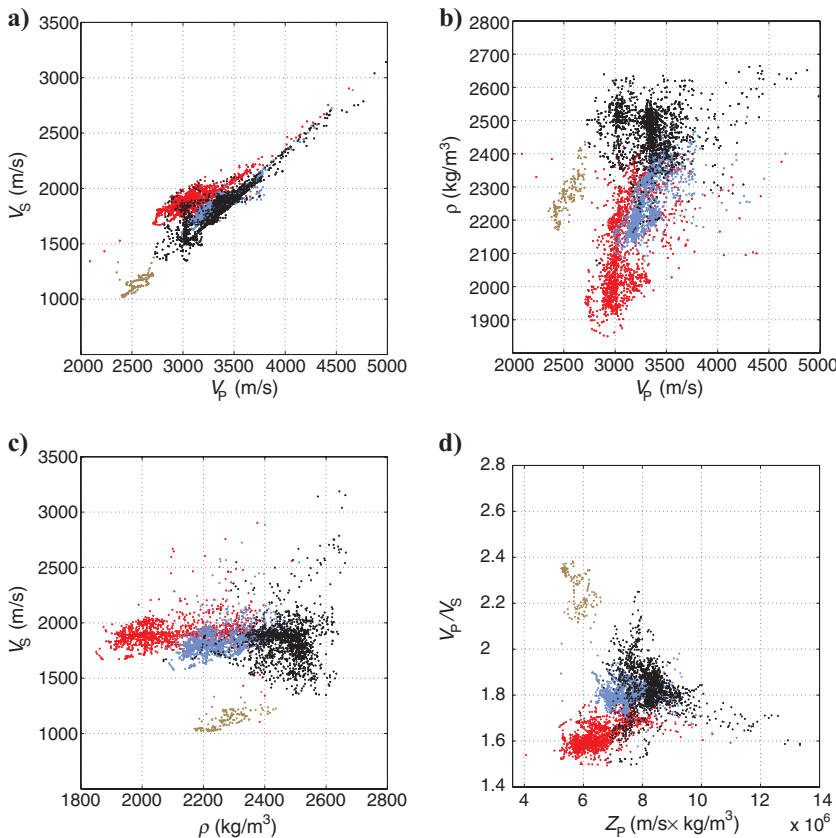


Figure 4. Elastic properties $\exp(\mathbf{m})$ represented by P-wave velocity V_p , S-wave velocity V_s , and density ρ , given gas-saturated sandstone (red), brine-saturated sandstone (blue), shale (black), and source rock (brown) from locationwise observations in two wells in (a), (b), and (c); and (d) impedance $Z_p = V_p \times \rho$ versus relative velocity V_p/V_s .

- 2) A locationwise prior model that ignores both vertical and horizontal dependence. In this model, we use spatially varying LF proportions.
- 3) A locationwise prior model with uniform probability for each of the LF classes. This corresponds to a maximum likelihood solution.

Posterior model

The approximate posterior model $\tilde{p}(\boldsymbol{\pi}|\mathbf{d})$, defined in [Ulvmoen and Omre](#) (this issue), is expressed through $\tilde{p}(\boldsymbol{\pi}_x|\boldsymbol{\pi}_{-x},\mathbf{d}_x)$ for all x , which are fully specified by the parameters assessed in the previous sections. With the posterior model being defined on this conditional form, a block Gibbs algorithm is used to simulate from the posterior. An outline of the algorithm is as follows:

Simulation Algorithm

Initiate

Generate arbitrary $\boldsymbol{\pi}$

Iterate

Draw x uniform randomly

Generate $\boldsymbol{\pi}_x$ from $\tilde{p}(\boldsymbol{\pi}_x|\boldsymbol{\pi}_{-x},\mathbf{d}_x)$ by the upward-downward simulation algorithm

The simulation algorithm is fully defined in [Ulvmoen and Omre](#) (this issue). However, note that the simulation is made by a computer-efficient recursive algorithm vertically, while an iterative algorithm must be used horizontally.

To evaluate the convergence rate of the simulation algorithm, the algorithm is initiated from four extreme configurations of the LF classes containing one class only. The proportion of each LF class after each sweep of the algorithm is shown in Figure 7, with one sweep corresponding to one update of each profile in the target zone. We see that all realizations with initial extreme configurations have reached the same proportion within 1000 sweeps, which we define to be the burn-in period for convergence.

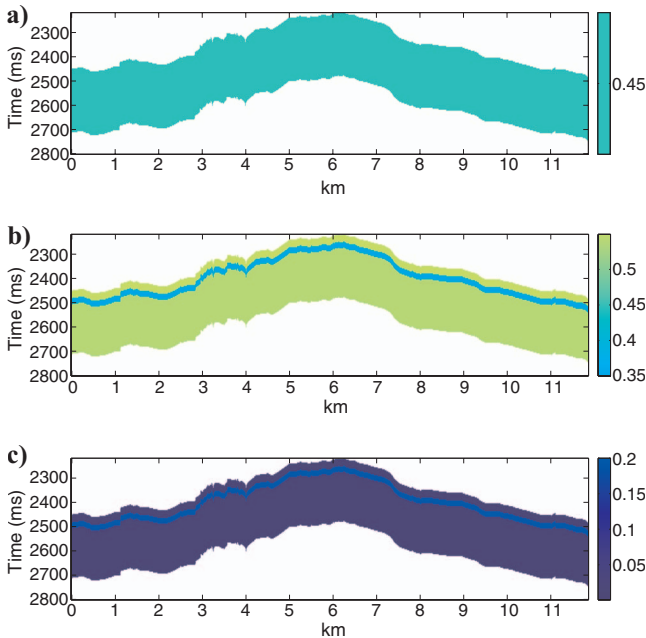


Figure 5. Expected proportions of the lithologies: (a) sandstone; (b) shale; and (c) source rock.

RESULTS WITH DISCUSSION

Our study focus is on LF characteristics, and realizations and prediction of these are obtained from the approximate posterior model. Realizations are generated from this posterior model, and the most probable prediction locationwise is calculated by counting the number of occurrences of each of the LF classes in each location, then choosing the LF class with most frequent occurrences. We use 400 realizations in this counting process, where the realizations are taken every 100 sweeps after burn-in.

Figure 8 contains three independent realizations from the approximate posterior model. These realizations can be considered as possible LF realities of the target zone, and they span the space of uncertainty. The structure is similar in the three realizations, the layers of lithology are elongated and thin, and the fluid gravity segregation is reproduced. Note that the well observations are exactly reproduced, and that they have lateral influence due to the horizontal dependence in the 2D Markov random field prior model. There is surprisingly little variability among the realizations. Assuming that the simulation algorithm has converged, this indicates that there is little prediction uncertainty given the current model with associated parameters. The

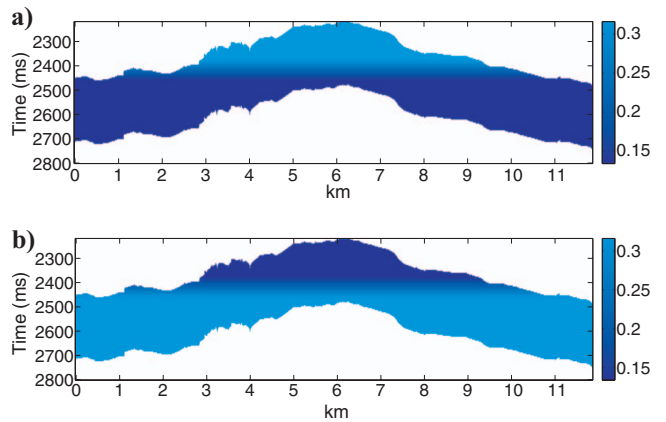


Figure 6. Expected proportions of (a) gas-saturated sandstone; and (b) brine-saturated sandstone.

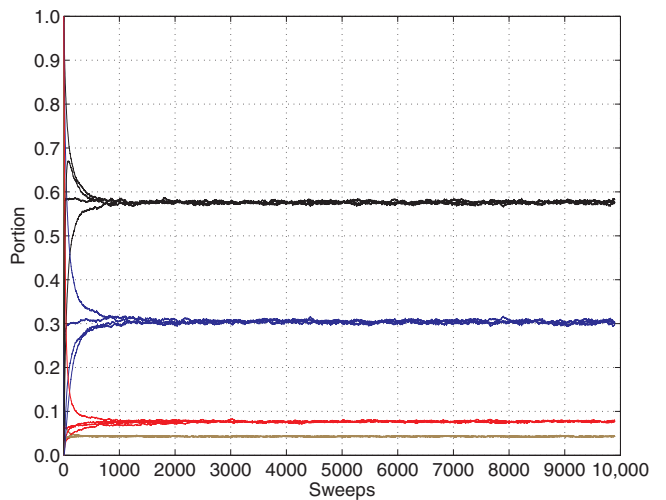


Figure 7. Convergence plot monitoring the proportion of LF classes after each sweep of the simulation algorithm.

uncertainty level is probably not fully representative for reservoir characterization in general since uncertainty in the model specification is not accounted for. These aspects require further research.

Figure 9 contains the LF class prediction based on the most probable class locationwise. The prediction has less spatial heterogeneity than the realizations, but not much so because the prediction uncertainty is small. The prediction appears as realistic with continuous, elongated lithology classes. The well observations are exactly reproduced, and due to lateral coupling, they have influence in the near-well region also. The seismic data seem to define the spatial pattern of the lithologies away from the well and the resolution in the inversion appears as good because many lithology units are thin. The proportion of the lithologies sandstone, shale, and source rock are approximately 0.37, 0.58, 0.05, compared to 0.45, 0.50, 0.05 in the well observations used in the prior model. The conditioning on seismic data is assumed to cause this change in proportions. The change is plausible because wells usually are preferentially located in good reservoir areas on top of structures. Consequently, sandstone proportions in wells tend to be higher than the reservoir average. Moreover, even sampling uncertainty of average proportions from well observations can cause these levels of deviations (see Ulvmoen and Omre, this issue). The gas is on top of brine as expected from gravity segregation, although the vertical trend of the prior fluid model probably is the major reason for this. We discuss impact of the prior fluid model later.

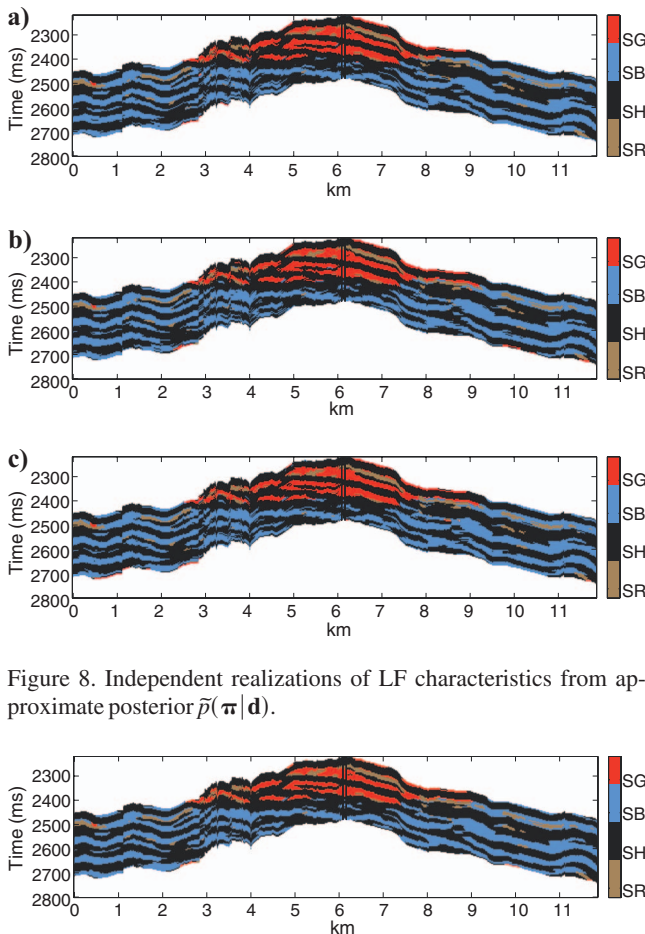


Figure 8. Independent realizations of LF characteristics from approximate posterior $\tilde{p}(\boldsymbol{\pi}|\mathbf{d})$.

Figure 9. Locationwise most probable LF characteristics prediction.

Figure 10 displays the LF-class prediction overlaying the manually interpreted layer geometry produced by the data owner. The layer borders seem to coincide reasonably well with lithology changes in the predictions. In structurally complicated areas around 4 km and before 8 km, the match is poorer because the concept of spatial continuity is unclear. The importance of automatic reproduction of layer geometries is primarily appreciated in 3D modeling, however.

Figure 11 contains the results from cross validation of the LF prediction in the well profile. The LF classes observed in the well are displayed along the left axis. The curves correspond to the marginal probabilities $\tilde{p}(\pi_{x,t}|\mathbf{d}^s)$ based on seismic data only. Fluid-filled sandstone is well reproduced. Some of the thinnest shales are merged and the source rock is slightly shifted. The latter is probably a consequence of the deconvolution. Cross-validation results look very encouraging and provide credibility to the LF prediction in Figure 9.

Figure 12 contains the LF-class prediction based on a 2D Markov random field prior model without a vertical trend in the prior model

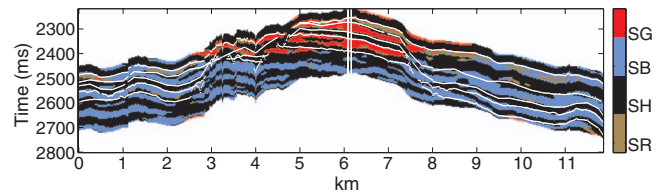


Figure 10. Locationwise most probable LF characteristics prediction overlayed by manually interpreted detailed layer geometry.

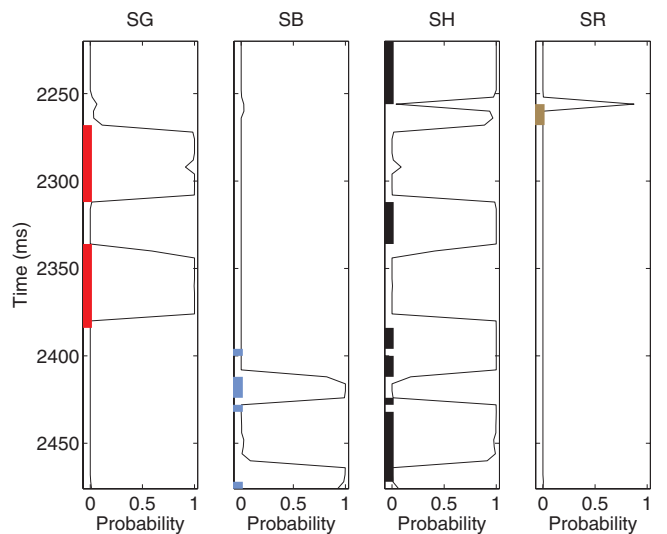


Figure 11. Marginal approximate posterior $\tilde{p}(\pi_{x,t}|\mathbf{d}^s)$ in well profile based on seismic data only, with well observations \mathbf{d}^w marked on each axis.

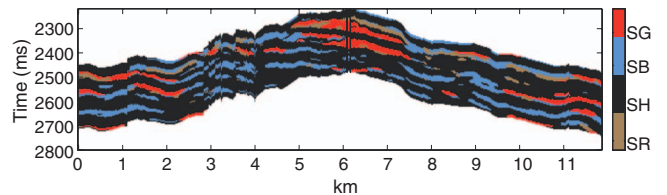


Figure 12. Locationwise most probable LF characteristics prediction based on a 2D Markov random field prior model without vertical trend in the fluid prior.

for the fluids. The prior model contains a stronger lateral dependence for gas than the previous model to compensate for the lack of fluid trends. The major gas volumes are predicted to be in the shallow parts of the reservoir where conditioning on well observations for gas has lateral influence. Pockets of gas also are predicted in deeper parts of the reservoir, however. Without lateral coupling in the prior model, the well observations of gas would stand out as a vertical gas column surrounded by brine.

Figure 13 contains realizations from the approximate posterior model from the four different prior models; the 2D Markov random field model, the profilewise Markov chain model, and the locationwise model with and without spatially varying LF proportions. These realizations reflect the spatial characteristics of the prior models. The spatially coupled 2D Markov random field prior model enforces continuity on the realizations, while locationwise prior models provide realizations dominated by the observation noise. It is obvious that the 2D Markov random field model generates realizations that are most geologically realistic.

Figure 14 contains the most probable predictions locationwise from the four prior models. The 2D Markov random field prediction is discussed above. The profilewise Markov chain prediction gives a good indication of the LF classes in the target zone. The prediction is calculated very quickly because the approximate posterior model is calculated analytically in each profile using a recursive algorithm.

Considering the prediction as a whole, there is a slight skyline ef-

fect due to lack of lateral continuity; hence the solution does not appear as realistic. Moreover, the well observations do not have an influence in their neighborhood due to lack of lateral coupling. The predictions based on locationwise prior models are extremely fast to compute. The prediction based on spatially varying prior proportions of LF classes clearly reflects this prior model, and seismic data appears to carry information concerning sandstone versus shale and source rock. Brine appears immediately above gas in some places, violating gravity segregation rules, however. Moreover, the lithologies appear as unrealistically patchy due to the influence of seismic noise and lack of lateral coupling in the model. The prediction based on the uniform LF proportion prior model reflects mostly the information content in the seismic data, though the well observations are used in the wavelet estimation and the rock-physics model. Note that the gas column observed in the well stands out surrounded by brine. However, even this prediction does reflect major characteristics of the lithology distribution.

Realizations and predictions in Figures 13 and 14, under different prior models, demonstrate that the 2D Markov random field reproduces the expected spatial pattern best due to lateral coupling in the prior model. Moreover, the well observations are given lateral influence under this prior model.

Figure 15 contains the marginal approximate posterior probability for the four prior models in the well profile, with the well observations marked on the axis. The prediction in this figure is made with-

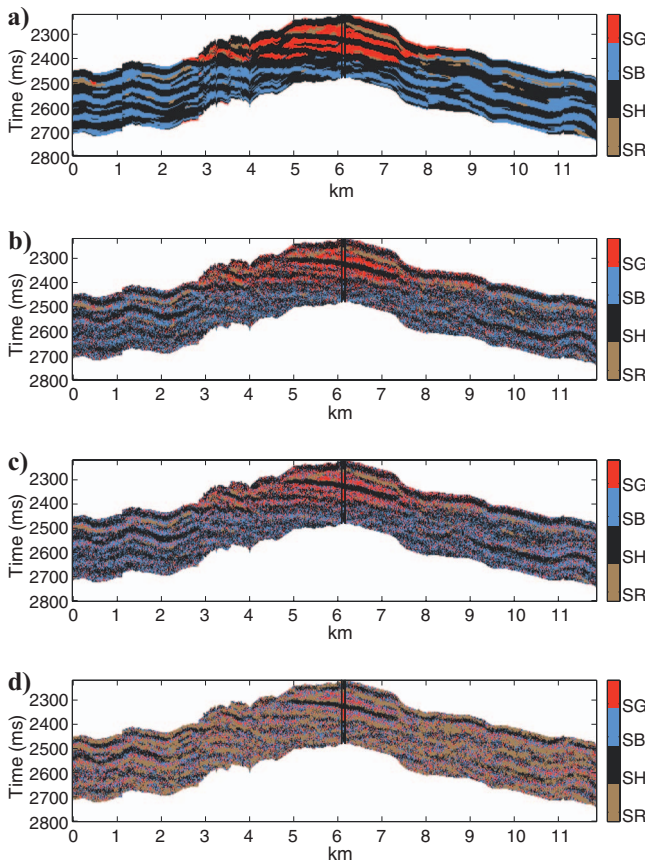


Figure 13. Realizations of LF characteristics from approximate posterior $\tilde{p}(\boldsymbol{\pi} | \mathbf{d})$ for (a) 2D Markov random field model; (b) profilewise Markov chain model; (c) locationwise model with depth-varying prior; and (d) locationwise model without depth-varying prior.

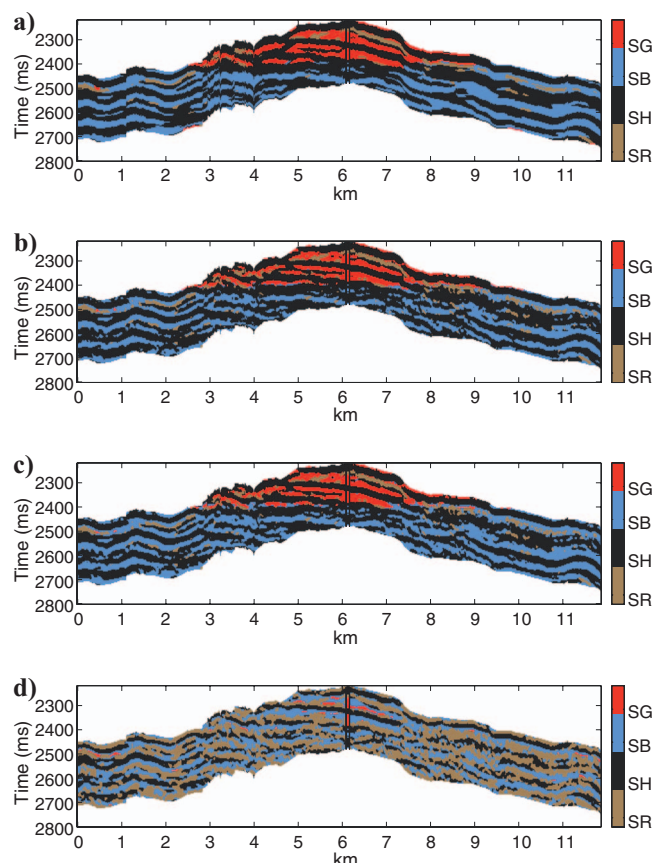


Figure 14. Locationwise most probable LF characteristics predictions for (a) 2D Markov random field model; (b) profilewise Markov chain model; (c) locationwise model with depth-varying prior; and (d) locationwise model without depth-varying prior.

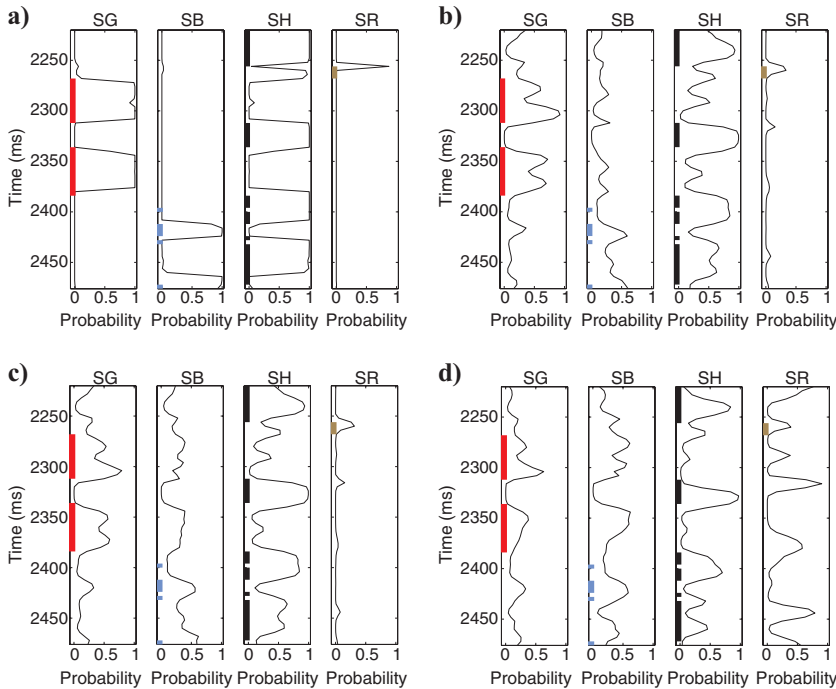


Figure 15. Marginal approximate posterior $\tilde{p}(\pi_{x,t} | \mathbf{d}^w)$ in well profile for (a) 2D Markov random field model; (b) profilewise Markov chain model; (c) locationwise model with depth-varying prior; and (d) locationwise model without depth-varying prior, with well observations \mathbf{d}^w marked on each axis.

out conditioning on the well data; hence in a cross-validation mode. The marginal probability profile appears as very conclusive and largely correct for the 2D Markov random field model. The other marginal probability profiles appear as much more diffuse — more so for models without spatial couplings. This demonstrates the importance of lateral coupling in the prior model, such that neighboring seismic profiles are jointly interpreted when identifying LF classes expected to have long lateral continuity.

CONCLUSIONS

LF inversion in a Bayesian setting is demonstrated on real seismic data from a sandstone gas reservoir offshore Norway. The general experiences from the study are as follows:

The general reservoir experience about LF horizontal continuity and vertical sequencing combined with spatial LF proportion adjustment, introduced through the profile Markov random field prior model, makes the inversion results look more geologically credible.

The approximate deconvolution approach for prestack seismic data appears as very reliable. Jointly with the horizontal coupling in the prior model, this approximation makes it possible to identify lithology units that are very thin.

Well observations are crucial for inference of the likelihood model. Note, however, that only global likelihood parameters are estimated; hence we try to avoid overfitting. In the conditioning, well observations are given spatial influence due to spatial coupling in the prior model.

Posterior LF realizations and prediction compare well with manual interpretations of reservoir layers. Moreover, cross validation of LF classes in the well reproduces the well observations very precisely, probably due to horizontal coupling in the model.

The inversion is performed under different choices of prior models. However, all the inversions are based on the approximate deconvolution approach. The realizations and prediction from the 2D Markov random field prior model compare favorably with results based on other prior models. More realistic continuity in LF variables is observed, and thinner units are identified. Uncertainty in the inversion represented by the set of realizations from the posterior model could be undervalued. This is probably caused by the model parameters being considered known as their estimated values. Introduction of model-parameter uncertainties would be a natural extension of the work.

The study is performed in a 2D cross section of the reservoir with 950 nodes horizontally and 65 nodes vertically. The study required approximately eight hours of computing time on an average-size sequential computer processor. Full 3D studies are well within reach because the algorithm runs linearly in the number of nodes, although the convergence rate can be somewhat lower in 3D couplings. Moreover, the block Gibbs simulation algorithm is well suited for parallelization.

ACKNOWLEDGMENTS

Our work was funded by the Uncertainty in Reservoir Evaluation (URE) initiative at the Norwegian University of Science and Technology (NTNU).

APPENDIX A

PARAMETERS IN GAUSSIAN MODEL

Variable \mathbf{m} contains the logarithm of the elastic material properties. The Gaussian probability $p_*(\mathbf{m})$ is parametrized by $(\boldsymbol{\mu}_*, \boldsymbol{\Sigma}_*, c_*(\tau))$ vertically, and the numerical values are estimated from the well using standard statistical estimators giving

$$\boldsymbol{\mu}_* = (7.99 \quad 7.36 \quad 7.75)$$

and

$$\boldsymbol{\Sigma}_* = \begin{pmatrix} 0.0106 & 0.0207 & 0.0012 \\ 0.0207 & 0.0506 & -0.0036 \\ 0.0012 & -0.0036 & 0.0051 \end{pmatrix},$$

with rows and columns corresponding to logarithm of P-wave velocity, S-wave velocity, and density, respectively, in units of m/s, m/s, and kg/m³. The temporal correlation function for P-wave velocity, S-wave velocity, the crosscorrelation between these, and the cross-correlations between S-wave velocity and density are given by a first-order exponential correlation function

$$c_*(\tau) = \exp\left\{-\frac{\tau}{d}\right\}$$

with range $d = 35$ ms. The remaining correlations are density and crosscorrelation between P-wave velocity and density. They are given by the weighted sum of a second-order exponential correlation function and a normalized second derivative of a second-order exponential correlation function

$$c_*(\tau) = 0.5 \exp\left\{-\left(\frac{\tau}{d_1}\right)^2\right\} + 0.5\left(1 - \frac{2\tau^2}{d_2^2}\right) \exp\left\{-\left(\frac{\tau}{d_2}\right)^2\right\},$$

with ranges $d_1 = 7.5$ ms and $d_2 = 35$ ms, respectively. This correlation function exhibits a weak hole effect.

APPENDIX B

BASIC TRANSITION MATRICES

Basic transition matrices with limiting distributions in 2D Markov random field prior model are

$$\mathbf{P}_{SG,SG}^t = \begin{pmatrix} 0.9996 & 0 & 0.0002 & 0.0002 \\ 0.9994 & 0.0002 & 0.0002 & 0.0002 \\ 0.9994 & 0.0002 & 0.0002 & 0.0002 \\ 0.9994 & 0.0002 & 0.0002 & 0.0002 \end{pmatrix}$$

$$\mathbf{P}_{SG,SG} = (0.9995 \quad 0.0000 \quad 0.0002 \quad 0.0002)$$

$$\mathbf{P}_{SG,SB}^t = \begin{pmatrix} 0.9990 & 0 & 0.0005 & 0.0005 \\ 0.4998 & 0.4998 & 0.0002 & 0.0002 \\ 0.4998 & 0.4998 & 0.0002 & 0.0002 \\ 0.4998 & 0.4998 & 0.0002 & 0.0002 \end{pmatrix}$$

$$\mathbf{P}_{SG,SB} = (0.9980 \quad 0.0010 \quad 0.0005 \quad 0.0005)$$

$$\mathbf{P}_{SG,SH}^t = \begin{pmatrix} 0.4999 & 0 & 0.4999 & 0.0002 \\ 0.4998 & 0.0002 & 0.4998 & 0.0002 \\ 0.4998 & 0.0002 & 0.4998 & 0.0002 \\ 0.4998 & 0.0002 & 0.4998 & 0.0002 \end{pmatrix}$$

$$\mathbf{P}_{SG,SH} = (0.4998 \quad 0.0001 \quad 0.4998 \quad 0.0002)$$

$$\mathbf{P}_{SG,SR}^t = \begin{pmatrix} 0.4999 & 0 & 0.0002 & 0.4999 \\ 0.4998 & 0.0002 & 0.0002 & 0.4998 \\ 0.4998 & 0.0002 & 0.0002 & 0.4998 \\ 0.4998 & 0.0002 & 0.0002 & 0.4998 \end{pmatrix}$$

$$\mathbf{P}_{SG,SR} = (0.4998 \quad 0.0001 \quad 0.0002 \quad 0.4998)$$

$$\mathbf{P}_{SB,SB}^t = \begin{pmatrix} 0.3333 & 0 & 0.3333 & 0.3333 \\ 0.0002 & 0.9993 & 0.0002 & 0.0002 \\ 0.0002 & 0.9993 & 0.0002 & 0.0002 \\ 0.0002 & 0.9993 & 0.0002 & 0.0002 \end{pmatrix}$$

$$\mathbf{P}_{SB,SB} = (0.0004 \quad 0.9989 \quad 0.0004 \quad 0.0004)$$

$$\mathbf{P}_{SB,SH}^t = \begin{pmatrix} 0.0005 & 0 & 0.9990 & 0.0005 \\ 0.0002 & 0.4998 & 0.4998 & 0.0002 \\ 0.0002 & 0.4998 & 0.4998 & 0.0002 \\ 0.0002 & 0.4998 & 0.4998 & 0.0002 \end{pmatrix}$$

$$\mathbf{P}_{SB,SH} = (0.0002 \quad 0.4996 \quad 0.4999 \quad 0.0002)$$

$$\mathbf{P}_{SB,SR}^t = \begin{pmatrix} 0.0005 & 0 & 0.0005 & 0.9990 \\ 0.0002 & 0.4998 & 0.0002 & 0.4998 \\ 0.0002 & 0.4998 & 0.0002 & 0.4998 \\ 0.0002 & 0.4998 & 0.0002 & 0.4998 \end{pmatrix}$$

$$\mathbf{P}_{SB,SR} = (0.0002 \quad 0.4996 \quad 0.0002 \quad 0.4999)$$

$$\mathbf{P}_{SH,SH}^t = \begin{pmatrix} 0.0002 & 0 & 0.9996 & 0.0002 \\ 0.0002 & 0.0002 & 0.9994 & 0.0002 \\ 0.0002 & 0.0002 & 0.9994 & 0.0002 \\ 0.0002 & 0.0002 & 0.9994 & 0.0002 \end{pmatrix}$$

$$\mathbf{P}_{SH,SH} = (0.0002 \quad 0.0002 \quad 0.9993 \quad 0.0002)$$

$$\mathbf{P}_{SH,SR}^t = \begin{pmatrix} 0.0002 & 0 & 0.4999 & 0.4999 \\ 0.0002 & 0.0002 & 0.4998 & 0.4998 \\ 0.0002 & 0.0002 & 0.4998 & 0.4998 \\ 0.0002 & 0.0002 & 0.4998 & 0.4998 \end{pmatrix}$$

$$\mathbf{P}_{SH,SR} = (0.0002 \quad 0.0002 \quad 0.4998 \quad 0.4998)$$

$$\mathbf{P}_{SR,SR}^t = \begin{pmatrix} 0.0002 & 0 & 0.0002 & 0.9996 \\ 0.0002 & 0.0002 & 0.0002 & 0.9993 \\ 0.0002 & 0.0002 & 0.0002 & 0.9993 \\ 0.0002 & 0.0002 & 0.0002 & 0.9993 \end{pmatrix}$$

$$\mathbf{P}_{SR,SR} = (0.0002 \quad 0.0002 \quad 0.0002 \quad 0.9993),$$

with rows and columns appearing in this order: gas-saturated sandstone, brine-saturated sandstone, shale, and source rock. Subindices on \mathbf{P}^t indicate the neighboring class.

The average of the basic transition matrices, used as transition matrix in the profilewise Markov chain model is

$$\mathbf{P} = \begin{pmatrix} 0.33 & 0 & 0.33 & 0.33 \\ 0.25 & 0.25 & 0.25 & 0.25 \\ 0.25 & 0.25 & 0.25 & 0.25 \\ 0.25 & 0.25 & 0.25 & 0.25 \end{pmatrix},$$

with associated limiting distribution

$$\mathbf{p} = (0.27 \quad 0.19 \quad 0.27 \quad 0.27).$$

APPENDIX C

ADJUSTMENT OF MARGINAL PROPORTIONS

Consider a stationary Markov chain with $(n \times n)$ -transition matrix

$$\mathbf{P} = \begin{pmatrix} p_{11} & \cdots & p_{1n} \\ \vdots & \ddots & \vdots \\ p_{n1} & \cdots & p_{nn} \end{pmatrix},$$

with $\sum_j p_{ij} = 1$ and limiting distribution $\mathbf{p} = (p_1, \dots, p_n)$ defined by $\mathbf{p} = \mathbf{P}^T \mathbf{p}$. The challenge is to adjust \mathbf{P} to have limiting distribution $\mathbf{q} = (q_1, \dots, q_n)$.

APPROXIMATION

Define

$$\mathbf{P}_q = \begin{pmatrix} \alpha_1 p_{11} q_1 / p_1 & \cdots & \alpha_1 p_{1n} q_n / p_n \\ \vdots & \ddots & \vdots \\ \alpha_n p_{n1} q_1 / p_1 & \cdots & \alpha_n p_{nn} q_n / p_n \end{pmatrix}$$

with

$$\alpha_i = (p_{i1} q_1 / p_1 + \cdots + p_{in} q_n / p_n)^{-1}.$$

The limiting distribution for \mathbf{P}_q is denoted $\mathbf{r} = (r_1, \dots, r_n)$ and defined by $\mathbf{r} = \mathbf{P}_q^T \mathbf{r}$. Hence, in the general case, $\mathbf{r} \neq \mathbf{q}$. Note, however, that \mathbf{P}_q will inherit extreme elements 0 and 1 from \mathbf{P} ; but otherwise the transition probabilities will be adjusted.

SPECIAL CASES

Case I: Extreme events

Events with $q_i = 0$ or $q_i = 1 \Rightarrow r_i = 0$ or $r_i = 1$. Thus extreme events will be reproduced.

Case II: Representative events

Consider $\mathbf{q} = (p_1, \dots, p_n) \Rightarrow \alpha_i = 1 \Rightarrow \mathbf{P}_q = \mathbf{P} \Rightarrow \mathbf{r} = (p_1, \dots, p_n) = \mathbf{q}$. Thus if \mathbf{q} coincides with \mathbf{p} , \mathbf{q} will be correctly reproduced.

Case III: Independence Markov chain

Consider

$$\mathbf{P} = \begin{pmatrix} p_1 & \cdots & p_n \\ \vdots & \ddots & \vdots \\ p_1 & \cdots & p_n \end{pmatrix} \Rightarrow \mathbf{P}_q = \begin{pmatrix} q_1 & \cdots & q_n \\ \vdots & \ddots & \vdots \\ q_1 & \cdots & q_n \end{pmatrix}$$

$$\Rightarrow \mathbf{r} = (q_1, \dots, q_n).$$

Thus if \mathbf{P} defines an independence Markov chain, \mathbf{q} will be reproduced.

Closing remark

The approximation reproduces extremes and has reliable approximations if \mathbf{p} and \mathbf{q} are not too different and/or the dependence in the Markov chain is weak.

REFERENCES

- Avseth, P., T. Mukerji, and G. Mavko, 2005, Quantitative seismic interpretation: Applying rock physics tools to reduce interpretation risk: Cambridge University Press.
- Bosch, M., C. Carvajal, J. Rodrigues, A. Torres, M. Aldana, and J. Sierra, 2009, Petrophysical seismic inversion conditioned to well-log data: Methods and application to a gas reservoir: *Geophysics*, **74**, no. 2, O1–O15.
- Buland, A., O. Kolbjørnsen, R. Hauge, Ø. Skjæveland, and K. Duffaut, 2008, Bayesian lithology and fluid prediction from seismic prestack data: *Geophysics*, **73**, no. 3, C13–C21.
- Buland, A., and H. Omre, 2003a, Bayesian linearized AVO inversion: *Geophysics*, **68**, 185–198.
- , 2003b, Bayesian wavelet estimation from seismic and well data: *Geophysics*, **68**, 2000–2009.
- Contreras, A., C. Torres-Verdin, W. Chesters, K. Kvien, and M. Globe, 2005, Joint stochastic inversion of petrophysical logs and 3D pre-stack seismic data to assess the spatial continuity of fluid units away from wells: Application to a Gulf-of-Mexico deepwater hydrocarbon reservoir: 46th Annual Logging Symposium, Society of Professional Well Analysts, Paper UUU.
- Eidsvik, J., P. Avseth, H. Omre, T. Mukerji, and G. Mavko, 2004, Stochastic reservoir characterization using prestack seismic data: *Geophysics*, **69**, 978–993.
- González, E. F., T. Mukerji, and G. Mavko, 2008, Seismic inversion combining rock physics and multiple-point geostatistics: *Geophysics*, **73**, no. 1, R11–R21.
- Ulvmoen, M., and H. Omre, 2009, Improved resolution in Bayesian lithology/fluid inversion from prestack seismic data and well observations, Part I — Methodology: *Geophysics*, this issue.